

STUDY ON FRACTURE PARAMETERS OF SELF-COMPACTING CONCRETE

By

VIJAYAKUMAR HALAKATTI*

*Department of Civil Engineering, Smt. Kamala and Shri. Venkappa. M. Agadi College of Engineering and
Technology (SKSVMACET) LAKSHMESHVAR-582116, Dist: Gadag, Karnataka State, India

Email: vijayakumar.civil@agadiengcollege.com

Abstract: This paper evaluates the fracture and material properties of self-compacting concrete (SCC) derived from the various non-linear fracture models from experiments through the three point bending tests on a series of geometrically similar beams. Using these properties as input data, computer simulation is performed using ATENA software by both smeared and discrete crack approach. A good agreement is observed between the experimental load-CMOD curves and the curves predicted by simulation. The total fracture energy G_F , critical crack tip opening displacement determined ($CTOD_c$) by RILEM and the stress intensity factor (K_{IC}) determined by LEFM principle are found to be size dependent where as K_{IC} and initial fracture energy (G_f) determined by RILEM are found to be material dependent properties. The size independent fracture energy is evaluated for SCC by tail end correction method. The influence of size effect and brittleness in SCC beams are identified. A bilinear crack model is proposed for SCC with a kink point. Efforts were made to link the fracture parameters of SCC to the proposed model. The co-ordinate of kink point such as stress ratio Ψ is directly calculated. Efforts are made to correlate the propagation of the cracks captured at increased loads during tests and simulation process on beams.

Keywords: Self compacting concrete, fracture parameters, simulation, kink point, bilinear model, size effect, brittleness.

I. INTRODUCTION:

Concrete is a quasi-brittle material of low strain capacity. The Linear Elastic Fracture Mechanics (LEFM) principles (Griffith theory) applied to brittle material are unsuccessful to the concrete due to the presence of pores, micro cracks of the order of a meter and discontinuities that lead to the softening response in the concrete. The size of the damage zone generally termed as fracture process zone (FPZ) is large as compared with the size of the small structure and is negligible in case of the large structures such as dams. Hence the validity of LEFM for concrete material is limited to large structures. In order to overcome this, several non-linear fracture mechanics (NLFM) models are developed by many investigators. These models introduce some material and fracture properties regardless of the structural geometry and the size.

Fracture mechanics theories promise better predictions about the life and durability of a structure in the presence of cracks. The problem to the researchers is the distributed cracking, softening in tension, size effect and brittleness. Many researchers identified these problems earlier. Even then, there is a need to investigate these factors especially the size effect because the present experimental evidence is more essential than that available from the previous literature.

The characterization of the softening curve from experimental load-CMOD curve is essential for the fracture behavior of quasi-brittle material such as SCC since it is different from the conventional cement concrete due to more powder in it. It is the concrete for structural elements with heavy reinforcements. Crack model is to be proposed from load-CMOD curves obtained by testing notched beams of geometrically similar sizes through three point bending test using very stiff servo hydraulic deflection controlled machine and clip gauges and later efforts can be made to link the various fracture parameters to this model. The experimental load-CMOD curves can be predicted by numerical simulation using FEM based ATENA software. The crack model proposed will be helpful to determine how much energy is required by the material before it fails by cracking.

The study is further extended to identify the size effect and brittleness. The codes on design of concrete structures are only empirical and do not count the size effect. These shortcomings of the code can be fully overcome by using the fracture mechanics approach.

II. RESEARCH SIGNIFICANCE:

This paper seeks to focus on the application of the fracture mechanics concept to the cracking, damage and fracture of concretes such as self-compacting concrete (SCC). The implementation of the mode-I fracture properties

of SCC in a crack model has been discussed. An attempt has been made to correlate the experimental curves with the model predictions using finite element method (FEM) based ATENA software. There is a need to identify the size effect, ductility (or brittleness) and the influence of size of SCC beams on the total fracture energy (G_F) and other fracture parameters. This will pave the way to modify the strength formulae used in the present codes. Using the fracture parameters of SCC as input data in the software, the structures of chosen dimensions such as pipes, dams and reinforced deep beams, corbels and portal frame can be simulated using ATENA software for the crack propagation, failure mode, and strength and ductility performances. This could help the designer to review his structural design.

III. LITERATURE REVIEW:

A. On Fracture Models:

Kaplan initiated the investigation on fracture mechanics of concrete only after 1960. Concrete is a quasi-brittle material. To overcome LEFM limitations, Hillerborg modified the cohesive crack model developed earlier by Barenblatt and Dugdale. The total fracture energy G_F as proposed by Hillerborg [1] (Shah et al., 1995) is a material property instead of the critical strain energy release rate G_C since, the G_F is based on the energy absorption and crack formation in the same place. The G_C is a material fracture constant used for the linear elastic material and brittle material.

The total fracture energy G_F is derived from fictitious crack model. It is the ratio of work of fracture (W_F) and un-cracked ligament cross sectional area. It is fracture energy averaged by the whole ligament area at crack front which includes both areas within and outside the fracture process zone (FPZ). The total fracture energy is represented by the area under the entire softening curve (w). Further, the variation of the total fracture energy with specimen size [2] (Raghu Prasad, 1996) has been observed by Gettu et al (1990), Wittmann et al (1990) and Hillerborg (1985).

In an alternative method proposed by Bazant and Pfeifer [1] (Shah et al., 1995), the fracture energy is determined from the size effect law which is known as the initial fracture energy (G_f). It is the critical energy release rate (G_f) which is a material fracture parameter obtained from Size Effect Model (SEM) or Two Parameter Fracture Model (TPFM). The advantage of providing this parameter is that it is size and shape independent. Hence it is the material dependent property. It represents the fracture energy which is area under initial tangent of the softening curve. It represents the fracture energy dissipated on a unit crack area in the FPZ. Of all the three values of fracture energies, the G_f and G_{IC} values are comparable. However, the value of G_F is approximately twice as great as the values of G_f and G_{IC} .

A bilinear crack model [3] (Jeffrey Roesler et.al 2007) was proposed earlier to a conventional concrete mix with fly ash of compressive strength 58.3 MPa. The Load (P)-CMOD curves obtained through the tests under deflection control system on geometrically similar beams as per RILEM under 3-point loading was perfectly fit with those by simulation using ABAQUS software.

The mean of peak loads for these companion beams from experimental load CMOD curves were 6.70 KN, 4.12 KN and 2.52 KN respectively. The total fracture energy G_F as determined by work of fracture method is a size dependent property and varies from 167 N/m for larger size to 119 N/m for smaller size. Further, the initial fracture energy G_f was 52.1 N/m and fracture process zone length (c_f) was 24.36 mm. The size effect was identified by size effect model (SEM) method.

The majority of cohesive crack models require a pre-defined crack path. It is supplemented by providing a groove at the centre of the beam under 3-point loading. It also requires penalty stiffness ($\frac{P_U}{w_{cr}}$) prior to softening curves. In softening curve, the penalty stiffness is the ratio of ($\frac{f_t}{w_{cr}}$). Crack initiation condition is commenced when the maximum stress in concrete reaches the tensile stress f_t of any concrete. Earlier to this stage, the penalty stiffness ($\frac{f_t}{w_{cr}}$) is created with full of micro cracks. In this state $f_t = f_{cohesive\ law}(w_{cr})$.

The area under the initial slope of the softening curve is the initial fracture energy G_f and controls the maximum load coming on the structures and hence the size effect. This can be determined by the procedures given in Size Effect Model (SEM) or from TPFM using the relation ($G_f = \frac{K_{IC}^2}{E}$) where K_{IC} is the critical stress intensity factor. This represents is the peak load of the specimen. The area under the tail of softening curve characterizes the post-peak load behavior which is given by the difference of total fracture energy (G_F) and initial fracture energy (G_f) i.e ($G_F - G_f$).

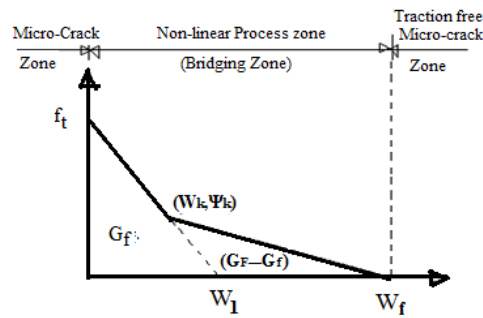


Fig1: Bilinear softening model based on experimental results

The co-ordinates of softening curve are specified by f_t , w_1 , w_f , Ψ and w_{cr} . However the ratio of $\frac{f_t}{w_{cr}}$ (penalty stiffness) is fixed for a particular concrete material. So only two unknowns such as w_1 and w_f are required and are evaluated as follows. The bilinear softening model³ as developed by the investigators is shown in **Fig 1** above.

$$\text{From this Fig, } w_1 = \frac{2G_f}{f_t} \quad \text{and} \quad w_f = \left(\frac{2}{\Psi f_t}\right) (G_F - (1 - \Psi)G_f) \quad (1)$$

Further investigations [3] reveal that the parameters G_f , f_t and Ψ at the kink point are material dependent property whereas G_F is size dependant property.

In continuation of this work [4] (Jeffrey Roesler et al., 2008), the kink point of the crack opening width (w_k) was hypothesized to $CTOD_c$. Hillerborg and Wittman determined a bilinear softening curve with the stress ratio at the crack point is 0.25. The value of the Ψ at kink point generally varies from 0.15 to 0.33. These four fracture parameters were linked to the bilinear softening curve as earlier.

$$\text{Referring the above Fig 1, Hypothesizing, } w_k = CTOD_c, \quad \Psi = \left[1 - \left(\frac{CTOD_c f_t}{2G_f}\right)\right] \quad (2)$$

The fracture process of plain concrete and rubberized concrete was investigated [5] (Chao Wang et al., 2012) by testing the beams under three-point bending tests. Later, simulation of the experimental softening curves is performed by ABAQUS software. It is found that the simulated P-CMOD curves agreed with the real test data. A bilinear fictitious crack model is proposed. It is also investigated that G_F increases with increase in strength of concrete.

It is investigated [6] (Planas et al., 2003) that the cohesive crack has proved to be excellent tool to describe the effect of notches on the strength of structural component.

Further, it is investigated [7] (Ricardo et al., 2006) that the ratio of $\left(\frac{G_F}{G_f}\right)$ was found to be 2.88 for specimen cast with the same concrete with the co-efficient of variation of 38.1%. These values comply with that given by Bazant and Beeq-Giraudon. The G_F increases as the compressive strength increase. The high performance concrete (HPC) should be designed using non-linear fracture mechanics.

The total fracture energy (G_F) can be determined by using load- CMOD curves or load deflection curves. The correction factors [8] (Apparao and Raghuprasad 2002) to account for variation in this quantity calculated by any one method depends on span/depth ratios. For beams with this ratio equal to 4, the ratio of energy as calculated for load deflection to load CMOD curve was 0.815.

The size effect [9] (Cervenka and Pukl, 1995) in concrete is studied using the computer program SBETA assuming that the material model is based on damage concept and smeared crack approach which is based on crack band theory. The experimental parameters obtained by JCI Round Robin for normal concrete were used as INPUT data in the ATENA software for all geometrically similar beams.

It is identified [10] (Zhifang et al., 2008) that the fracture energy increases with increase in specimen size and increase in maximum aggregate size.

B. Mix Design for Self Compacting Concrete (SCC)

Self-Compacting Concrete (SCC) is different from the normal concrete as it contains more powder and sand than the coarse aggregates. SCC has to satisfy the stages such as self-compaction when it is fresh whereas strength and durability at hardened state. Self-compaction is achieved by using super plasticizer, limited aggregate content whereas strength and durability by using low w/c ratio, limiting the coarse aggregates content.

An empirical method [11] (Okamura and Ozawa, 1994) known as rational method is earlier introduced. The guidelines [12] (EFNARC, 2002) given in EFNARC are based on this method. The method procedures are too complicated for practical implementation. The method uses large quantity of binders compared to the other mix designs and hence yields higher strength than that actually required. The method is suitable for gravelly rounded aggregates.

TABLE 1
MIX PROPORTION OF SCC

| Parameters:P.F-1.12, S/a ratio-5.5 | | | |
|---|--------------|-------------------------------------|------------|
| Material | Qty in kgs | Volume | Proportion |
| Cement | 450.00 | V_{cement} | 0.143 |
| Fly ash | 67.07 | $V_{Fly\ ash}$ | 0.054 |
| Powder | 517.07 | V_{powder} | 0.197 |
| Fine aggregate | 930.6 | $V_{Fine\ agg}$ | 0.364 |
| 20mm(20% of CA) | 149.04 | $V_{C.A}$ | 0.280 |
| 12.5mm(80% of CA) | 596.16 | $V_{Total\ agg}$ | 0.644 |
| Water in kgs after correction for SP | 163.26 | V_{water} | 0.144 |
| SP dosage (% of cement) | 1.2%(5.40kg) | V_{paste} | 0.341 |
| SP dosage(% of powder) | 1.05% | V_{mortar} | 0.705 |
| w/p ratio | 0.316 | $\frac{V_{mortar}}{V_{powder}}$ | 0.731 |
| Agg /cement ratio | 3.724 | $\frac{V_{mortar}}{V_{paste}}$ | 0.422 |
| | | $\frac{V_{total\ agg}}{V_{cement}}$ | 4.503 |

Method suggested by Nan Su et.al [13] (Nan Su et al., 2001) is based on packing theory. It starts with the packing of all aggregates and later with filling of aggregate voids with paste. This method is easier to carryout and yields less quantity of powder (mixture of cement and filler material) making concrete more economical. But it is more difficult to achieve satisfactory workability requirement at higher packing factors of 1.16 to 1.18 due to the less powder content. Of all the methods including the method such as Absolute volume method [14] (Nagendra and Sharadhabai 2013), the Nan Su method is more popular as it is simple to adopt.

EFNARC [15] recommends a series of test methods on fresh SCC such as slump/flow, U flow test, V-flow test, L-box test etc. It is investigated [15] (Manu Santhanam and Subramanian, 2004) that the mechanical properties of hardened SCC are similar to conventional concrete having equal w/c ratio. However, SCC is considered to be far superior due to better durability.

A mix design [16] (Vijayakumar and Shamu, 2015) for M50 strength is carried out by Nan-Su method using Ordinary Portland cement (OPC) of 53 grade and other ingredients with the material properties as given below. The fly-ash is used as the filler material. The Glenium B233, Poly corboxylated ether (PCE) based super-plasticizer is used as water reducer. The Mix Proportions of SCC are presented in Table 1 above.

TABLE2:
PROPERTIES OF FRESH SCC

| Properties | Range | Test Results |
|--------------------|-----------|--------------|
| Slump flow | 650-800mm | 690 mm |
| T ₅₀ cm | 2—5 sec | 3.0 sec |
| J-ring | 0—10mm | 5.8 mm |
| V-funnel | 8—12 sec | 8.8 sec |

| | | |
|--|----------|----------|
| V-funnel (5min) | +3sec | 11.2 sec |
| L-box(H ₂ /H ₁) | 0.8 –1.0 | 0.88 |
| U-box(H ₁ -H ₂) | 0—30 mm | 16 mm |
| Orimet | 0—5 sec | 3.0 sec |

TABLE 3
 PROPERTIES OF HARDENED SCC

| Properties | IS code | Results |
|-----------------------------|-------------|-----------|
| 7 days compressive strength | IS 516:1999 | 40.77 MPa |
| 28days compressive strength | | 56.16 MPa |
| Young's modulus | IS 516:1999 | 36700 MPa |
| Poisson's ratio | | 0.184 |
| Split tensile strength | IS5816:1999 | 4.19 MPa |

Workability requirement tests as suggested by EFNARC are performed on fresh mix and strength requirement on harden SCC. The tests results on fresh mix and hardened mix performed as per the procedure (IS.516-1999 and IS.5816-1999) are given in Table 2 and Table 3 respectively.

IV. EXPERIMENTAL INVESTIGATION:

A. Material Properties

Cement: Ordinary Portland cement of 53 grade of specific gravity 3.15 (Confirms with IS12269:1987).

Fly Ash: Class F dry fly ash of specific gravity 2.15 (Confirms to IS 3812–2003).

Fine Aggregates: River sand of specific gravity 2.56 and Fineness Modulus 2.78 and confirms to zone II (IS.383-1970). The bulk density is 1510.10 kg/m³ for loosely packed aggregates.

Coarse Aggregates: Crushed aggregates of sizes 20 mm and 12.5 mm in the proportions of 20% and 80% by weight respectively were used. Fineness Modulus (F.M) of the combined aggregates -7.086. Specific gravity-2.66. Bulk density - 1478.6 kg/m³ for loosely packed aggregates.

Water: Water suitable for drinking confirming to IS-3025-1983 (water for construction purpose) (IS 456-2000). Its pH value is 7.17.

Super Plasticizer: Glenium B 233, a PCE based that (Confirms to IS 9103-1999). It's pH value-6.82, Dry material content-34.51%.

Dosage of Super plasticizer: This is found by conducting Marsh cone test as per the procedure given in the literature [17] (Shetty, M.S., 2008). The optimum dosage of super plasticizer is 1.2% by weight of cement.

B. Provision of Beam Sizes:

These are determined as per RILEM Recommendations [1] (Shah, et al., 1995) and are given in Table 4. Maximum size of coarse aggregate $d_a = 20\text{mm}$. Notches (Grooves) in the beams can be made either by using saw-cut machine or can be made while casting. In this study, the notches of all specimens were saw cut, S/D ratio= 4 and $(\frac{a_o}{D})$ ratio=0.33.

TABLE 4
 DIMENSIONS OF SCC BEAMS IN MM

| Span(S) | Length (L) | Depth (D) | Thickness(t) | Notch depth (a_o) | Notch width |
|---------|------------|-----------|---------------|-----------------------|-------------|
| 960 | 1100 | 240 | 100 | 80 | 8 |
| 480 | 550 | 120 | | 40 | 6 |
| 240 | 275 | 60 | | 20 | 4 |

C Testing Arrangement

The beams are tested under three point bending employing the deflection controlled machine by carefully operating the machine in the laboratory. The arrangement of a beam for testing is shown in Fig 2 below.

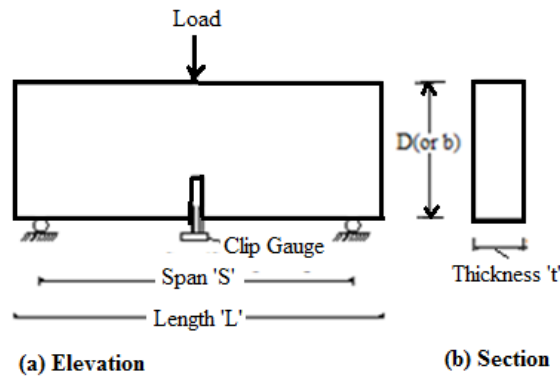


Fig 2: Three point testing arrangement for beam

The CMOD is measured by the clip gauge of maximum capacity of 10 mm, gauge length of 5mm, +2/-1mm measuring range at standard temperature range. Based on double cantilever design, RELIANT clip gauge features a full, 350 ohms, strain gauge Wheatstone bridge design. The equipment has 2 knife edges to mount inside cut groove. The linearity of the instrument is 0.20% of full measuring range for measurement greater than 6mm travel. The different stages of testing of beams in the laboratory are shown in Fig 3 below.



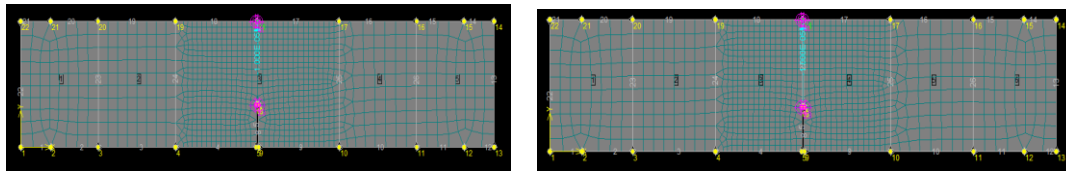
Fig3: Different stages of testing of beams

D. Software Used in the Research Work

The non-linear analysis of SCC beams is performed by using the finite element method (FEM) based ATENA software. The simulation [1] (Shah, et al., 1995) can be performed by Smeared or Discrete Crack Approach. The Smeared crack approach is based on the Bazant's crack band model. This is adopted where distributed cracking is possible. The crack is not straight but tortuous. The beam is divided with general linear elastic element known as bulk elements of rectangular shape. The bulk element employs two dimensional plane stress assumption to represent the linear elastic behavior in stage-I. Hence these elements have the stress-strain relationship governed by $\sigma_{bulk\ element} = f_{elastic}(\epsilon)$.

The Discrete Crack Approach is based on cohesive crack model in which crack path is assumed as priori and mesh with cohesive surface elements are arranged so that the path coincides with the boundaries between the bulk elements thereby bridging continuum between these two types of elements. This concept is best suited for notched beam under 3-point bending. These cohesive elements have the traction and separation relationship as $\sigma_{cohesive\ element} = f_{cohesive\ law}(w)$. The cohesive elements represents $f_{cohesive\ law}$ of crack initiation stage-II, later the non linear cohesive law represented by stage-III and finally failure criteria represented by stage-IV of fracture processes of concrete.

The ATENA software is based on smeared crack approach. It can also be used as discrete crack by introducing 2D interface where cracks are possible by introducing cohesive elements of desired properties following cohesive law. Simulation for softening curves is performed for full beam. The mesh is formulated by using four node quadrilateral bulk elements with 10 elements over the depth of beam and of total 1280 nodes and 960 elements for beams of each size by both the approaches as shown in Fig 4 (a) and Fig 4 (b) below.



(a) For smeared crack approach (b) For discrete crack approach

Fig 4: Arrangement of elements in beams

The crack model requires a unique tensile stress (σ) – crack width (w) relation to quantify the value of energy dissipation. The choice of σ - w function influences the prediction of structural response significantly and the local fracture behavior i.e. the crack opening displacement (COD) which is sensitive to the shape of σ - w curve. Many different shapes of σ - w curves have been proposed by Hillerborg. To simulate for the crack propagation and experimental monotonous load v/s CMOD curves, the ATENA software requires three important properties such as tensile stress (f_t) of SCC, total fracture energy (G_F) and evolution of failure (or the type of softening) in FPZ which describes the relation between tensile stress (σ) responsible for separating the crack v/s corresponding crack opening width (w) across the fracture surface. Along with these three quantities, the experimental material properties such as Young's modulus (E), Poisons ratio (μ), Cube strength (f_c) and Specific weight of SCC (ρ) are used as INPUT data. For simulation by discrete crack approach, the σ - w relation is defined by cohesive law whereas in case of smeared crack approach, exponential type of tension softening is used.

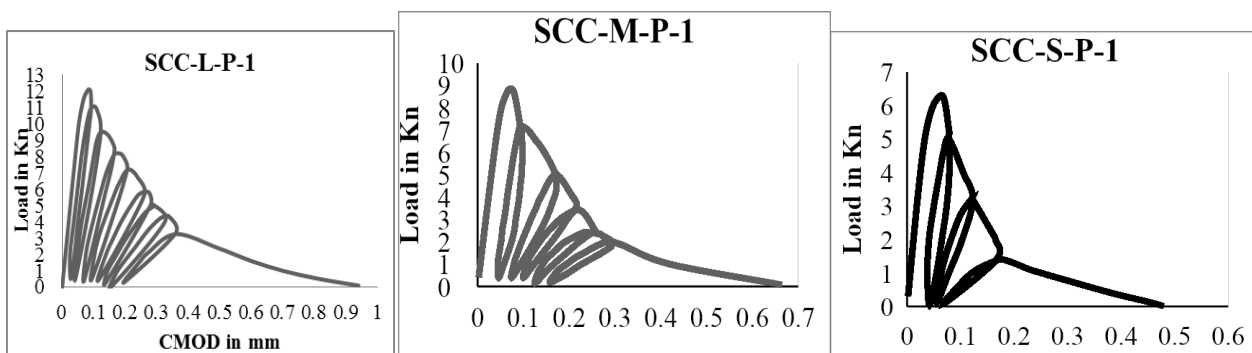
Two non-linear solution techniques are Standard Newton Raphson and Standard Arc Length methods. These can be modified with iteration numbers greater than 40 as required.

V.RESULTS AND DISCUSSIONS:

A. Determination of Fracture Parameters from Experiments and Simulation Curves

The loading and unloading cycles were obtained for the geometrically similar beams through the three point load tests using servo deflection controlled machine. The results with load CMOD cycles for some of the SCC beams such as Large size plain beam specimen no 1 (SCC-L-P-1), Medium size plain beam specimen no1 (SCC-M-P-1) and Small size plain beam specimen no1 (SCC-S-P-1) are shown in Fig 5(a), 5(b) and 5(c) respectively.

The loading and unloading slopes of the first cycle of graph of each beam specimen are used to determine the loading compliance (C_l) and unloading compliance (C_u). These compliances are further used to determine the Critical crack length (a_c), the fracture parameters such as Critical crack tip opening displacement ($CTOD_c$) and Critical stress intensity factor (K_{Ic}) under mode I of fracture that is derived from two parameter fracture mechanics (TPFM).model. To determine these values, the model needs at least one loading and unloading cycle, peak load (P_c) and self weight of the beam.

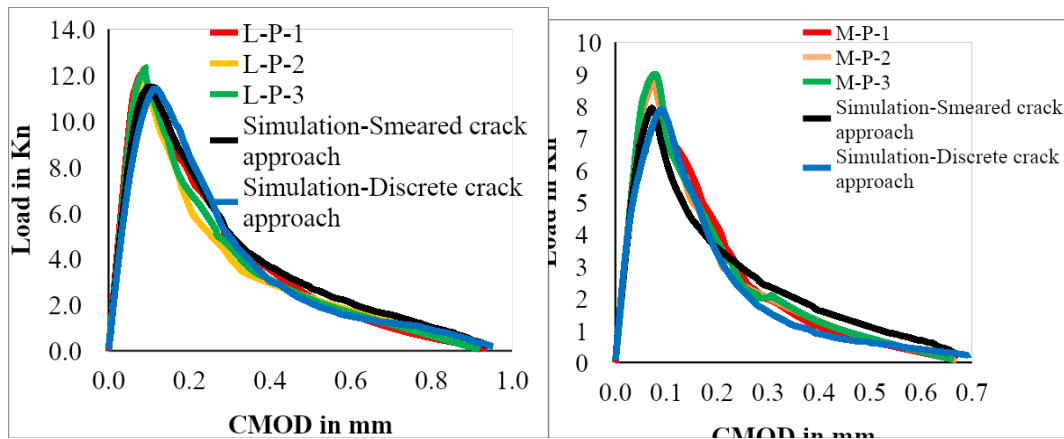


(a) For Large size beam sp-1 (b) For Medium size beam sp-1 (c) For Small size beam sp-1

Fig5: Load-CMOD cycles for all plain SCC beams

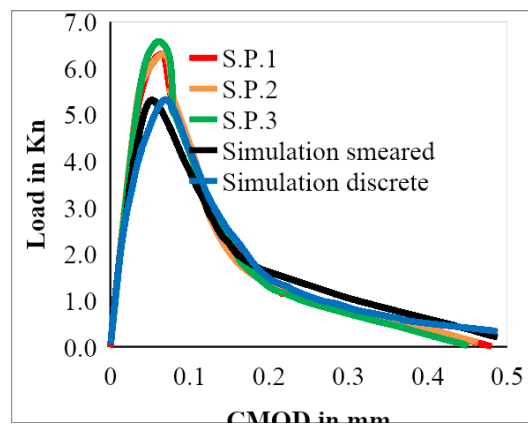
The overall failure envelope curves were developed by smoothly joining the peaks of all the cycles in experimental P-CMOD curves of the Fig 5. This is repeated for all companion beams of each size and compared with simulation curves that were obtained by both smeared and discrete crack approach as shown in Fig 6(a), (b) and (c) below.

The simulation is perform for all three geometrically similar beams using the respective experimental total fracture energy (G_F) along with type of tension softening and other material properties as input data in the software. The resulting load v/s CMOD from simulation are incorporated with experimental envelope curves in Fig 6 below.



(a) For Large size plain SCC beams

(b) For medium size Plain SCC beams



(c) For Small size Plain SCC beams

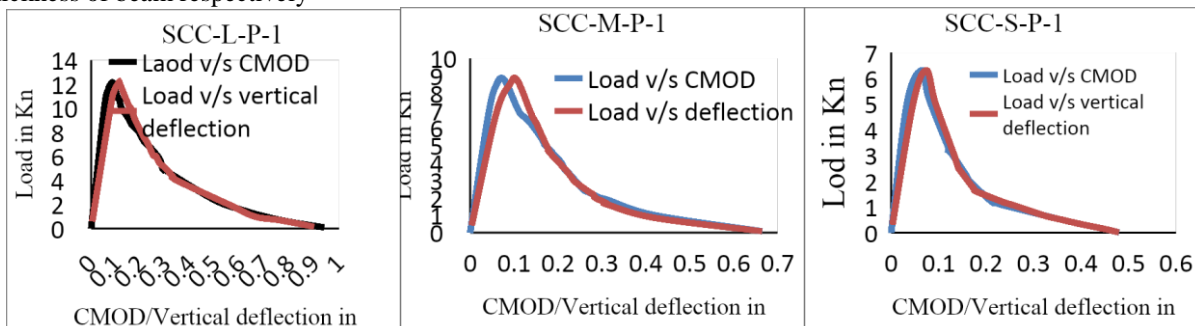
Fig 6: Comparison of experimental with simulation curves

The areas under all resulting experimental failure envelope curves of **Fig 6** are used to determine the total fracture energies using RILEM method of work of fracture method introduced by Hillerborg et al., [1](Shah, et al., 1995)

$$G_F = \frac{\text{Total energy}}{\text{Area of concrete fracture}} = \frac{W_f}{(D-a_o)t} = \frac{W_o + 2P_w\delta_o}{(D-a_o)t} \quad (3)$$

Where, W_o = Area under load – CMOD curve, P_w = Self weight of beam,

δ_o = The CMOD corresponding the raw load $P_a = 0$, and D, a_o and t are Depth of beam, notch depth and thickness of beam respectively



(a) For Large size beam sp no-1

(b) For Medium size beam sp no 1

(c) For Small size beam sp no 1

Fig7: Comparison of experimental load-CMOD with load-deflection curves for Plain SCC beams

It is observed from the **Fig 5** and **Fig 6** that as the size of the beam decreases, the peak load in P-CMOD curve decrease. This shows that the ductility of the specimen increases as the size of beam decreases. Thus the brittle fracture that occurs for large size beam will be transformed in to the ductile fracture for smaller beam.

Further, the overall envelope curves that were captured for load deflection during experiments are compared with that of obtained for load CMOD curves. The comparison for some of the specimens is shown in **Fig 7(a), (b)** and **(c)** above. It is observed from these figures that load CMOD curves are stiffer than load deflection curves at pre

peak load conditions and at higher loads at post peak load positions.

The load deflection envelope curves that were captured from experiments for some of beams such as L-P-1, M-P-1 and S-P-1 specimens were compared with the corresponding simulation curves obtained by the both the approaches and are shown in **Fig 8** below. These curves are further used to determine the total fracture energy (G_F) and compared with that obtained from load CMOD curves. These results are presented in **Table 6** below.

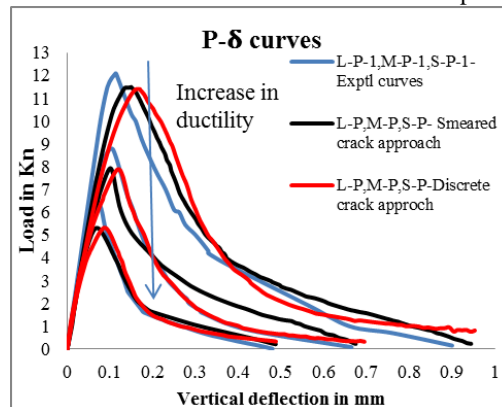


Fig8: Experimental load-deflection curves and simulation curves

C. Study of Crack Propagation in SCC Beams

It is observed while performing tests on the notched beams that the failure was initiated by the formation of a crack process zone with micro cracks in the region of tensile stress i.e. at the bottom of the notch. The first crack in the notch was initiated when the load reaches a range from 0.70 to 0.78 of the peak load for all the beams. When the load reaches the ultimate value, the separating stress σ reaches the tensile stress (f_t) of SCC. The crack width corresponding to this stage is the critical crack width (w_{cr}). The figures shown in **Fig 3** are captured while performing experiments and these will show the different stages of crack initiation and propagation for some of the beams.

Similarly, the initiation and propagation of cracks above the notch portion at different loads steps captured while simulation is performed is shown in **Fig 9.1** by smeared crack approach and in **Fig 9.2** by discrete crack approach below.

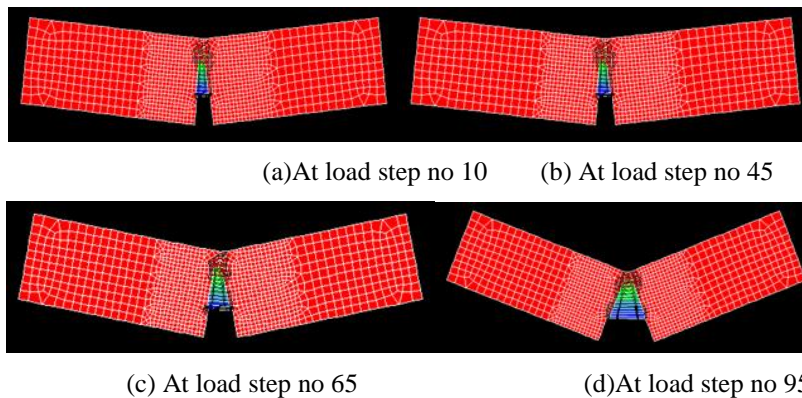


Fig 9.1: Cracks in notched beam by Smeared crack approach

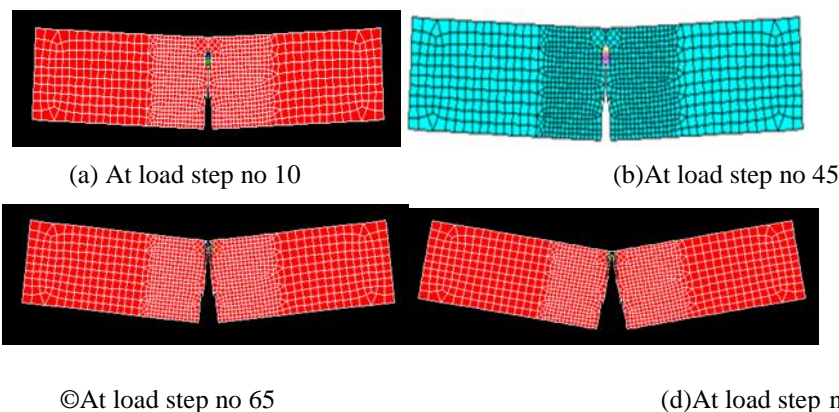


Fig 9.2: Cracks in notched beam by discrete crack approach

Efforts are made to correlate the propagation of cracks captured at various load steps during simulation shown in **Fig 9.2** with those captured during experiments as shown in **Fig 3**. The crack shown in **Fig 9.2 (d)** is captured at just few load steps before the total collapse of the beam. In this discrete crack, cohesive elements are introduced following cohesive law in the ligament just above notch. The either parts of the cracks still remains since the cohesive stress introduced in the ligament still are not being totally released. This is possible in the beam only through simulation. But practically, it is impossible to remain in this position since, SCC is brittle material compared to normal concrete. However, this crack shown in **Fig 9.2 (d)** can be considered analogous to the last slide of **Fig 3** where there is total failure of beam is occurred.

D. Determination of K_{IC} and $CTOD_c$ for SCC as per RILEM:

The K_I represents the stress intensity factor of concrete material. It can be calculated from LEFM principles. The structures of a given concrete material with different geometries and sizes are subjected to peak loads, then K_I and CTOD will be represented as K_{IC} and $CTOD_c$ respectively. At this condition, $G_{IC} = \left(\frac{K_{IC}^2}{E}\right)$ where G_{IC} is the critical energy release rate which represents the energy rate consumed during material fracturing in creating two surfaces which is equivalent to material surface energy. The G_{IC} and the initial fracture energy G_f are comparable since both are derived from effective elastic crack models. Thus, K_{IC} is used to determine G_{IC} . The other applications of K_{IC} and $CTOD_c$ are to determine the material length “Q” given by $\left(\frac{E \cdot CTOD_c}{K_{IC}}\right)^2$ which is material characteristic property given by Jenq and Shah, to estimate the theoretical tensile strength and to predict the critical fracture load for structures with different sizes and geometries. The parameters calculated as per the RILEM are given in **Table 5** below. It is found that the K_{IC} of SCC remains almost the same value with its value ranging from 57.98 to 60.44 MPa√mm for all beams and hence is the material dependent property.

The G_{IC} or G_f varies from 90.53 N/m to 98.59 N/m for all sizes and is identified to be a material dependent property.

TABLE 5
 FRACTURE PARAMETERS OF SCC

| Specimen ID | TPFM | | | | $G_f = G_{IC} = \left(\frac{K_{IC}^2}{E}\right)$ | |
|-------------|--------------------|---------|----------------|---------|--|---------|
| | K_{IC} in MPa√mm | CV In % | $CTOD_c$ In mm | CV In % | $G_f = G_{IC}$ in N/m | CV In % |
| L-P-1 | 58.49 | 0.62 | 0.0158 | 7.94 | 92.72 | 1.26 |
| L-P-2 | 57.980 | | 0.0145 | | 91.10 | |
| L-P-3 | 57.79 | | 0.0135 | | 90.53 | |
| M-P-1 | 58.92 | 1.41 | 0.0112 | 4.45 | 94.08 | 2.81 |
| M-P-2 | 60.32 | | 0.0122 | | 98.59 | |
| M-P-3 | 60.44 | | 0.0115 | | 98.997 | |
| S-P-1 | 59.04 | 0.54 | 0.0075 | 8.61 | 94.46 | 1.08 |
| S-P-2 | 59.68 | | 0.0081 | | 96.52 | |
| S-P-3 | 59.42 | | 0.0080 | | 95.67 | |

Earlier investigations show that both K_{IC} and $CTOD_c$ are material dependent properties which are constant for a particular concrete mix. But, the $CTOD_c$ of SCC mix decrease as the size of beam reduces. Hence, the $CTOD_c$ is size dependent property.

E. Determination of Stress Intensity Factor (K_{IC}) for SCC Considering Cohesive Forces:

In the above **Table 5**, the K_{IC} values are determined from RILEM procedure. However, this procedure is same as that suggested for the metal which is homogeneous material. SCC (or Concrete) is a heterogeneous material made of matrix (cement paste) and aggregates. Its heterogeneity increases with increase in size and volume of coarse aggregates. Concrete is generally accepted as homogeneous material before cracking if the minimum dimension of the beam is greater than five times of the maximum size of coarse aggregates used. It is identified that as the aggregate size increases, K_{IC} increases. Ohgishi et al.[18](**Karihaloo, 1995**) observed significant increase in K_{IC} for cement mortar than the hardened cement paste. H.Eskandari et al.[19] (**Eskandhari et al., 2010**) determined K_{IC} using basic LEFM expression which considers cohesive stresses in it. They used crushed granite aggregates of maximum size of 16 mm for 3 geometrically similar beams of depths 50,100 and 200mm considering the minimum size of 50mm greater than three times the maximum size of coarse aggregates (i.e. 3*16=48mm).

In this research, SCC is prepared with maximum size of 20mm. the depths of 3 beams with S/D ratio = 4 and ($\frac{a_0}{D}$) ratio =0.33 are 60,120 and 240mm considering uniform thickness of 100mm for all beams. But the depth of smaller 60 mm is less than (5*20) =100mm. This violates the requirement to consider SCC as homogeneous

material. However, for cement mortar, this requirement will be satisfied since dimensions of all beams are lesser than (5*4.75mm) 23.75mm. In such case, the K_{IC} value for SCC should be evaluated from the fundamental equation based on LEFM principle which considers the cohesive forces σ_c at critical state which occurs at peak load on notched beam and is considered to be equal to tensile strength (f_t) of SCC.

$$\text{i.e. } K_{IC} = \sigma_c \sqrt{\pi a_c} g_1 \left(\frac{a_c}{D} \right) \quad (4)$$

a_c =critical crack length, $g_1 \left(\frac{a_c}{D} \right)$ is the geometric factor for notched beam at critical state.

TABLE 6
 K_{IC} VALUES FOR BEAMS DUE TO COHESIVE FORCES

| Beam series | Dimensions in mm | $\sigma_c = f_t$ in MPa | Notch depth a_o in mm | Critical crack length (a_c) mm (Av) | Geometric function(Av) | K_{IC} in MPa \sqrt{mm} |
|-------------|------------------|-------------------------|-------------------------|---|------------------------|-----------------------------|
| L-P | 100*240*1100 | | 80 | 87.83 | 1.123 | 78.18 |
| M-P | 100*120*550 | 4.19 | 40 | 44.61 | 1.132 | 56.16 |
| L-P | 100*60*275 | | 20 | 22.16 | 1.128 | 39.44 |

D. Benarhia and Benguediab [20](Djamila, et al., 2015) evaluated K_{IC} for notched beams subjected to TPB using the above relation. Similarly, the values of K_{IC} are evaluated for SCC beams using above relation (4) in this research work and are presented in the Table 6 above.

It is observed from the above Table 6 that K_{IC} determined from LEFM will be size dependent property. The size of beam increases, the K_{IC} also increases. This property will comply with those of the investigations made by Rossi [18] (Karihaloo, 1995). In such case, the initial fracture energy $G_f = G_{IC}$ cannot be evaluated from the relation $\frac{K_{IC}^2}{E}$ since G_f is the material dependent property.

Refai and Swartz [1] (Shah, et al., 1995) identified that there will be variation of K_{IC} with different beam sizes. It is seen that when the when the beam depth varies from 50mm to 800 mm, the K_{IC} changes approximately by 30%. But, the K_{IC} is fairly constant, if the beam depth is greater than 400mm. Hence, it is generally agreed that the value of K_{IC} is essentially specimen size dependent.

F. Determination of Total Fracture Energy (G_F) as per RILEM Procedure

The experimental and simulation curves as shown in Fig 6, Fig 7 and Fig 8 are used to determine the total fracture energies and are presented in Table 7 below. The experimental G_F as calculated from load CMOD curves and material properties of SCC are used as input data for simulation using ATENA software and these results are given in the same Table 7 below.

TABLE 7
 COMPARISON OF TOTAL FRACTURE ENERGIES (G_F) AS FROM EXPERIMENTS AND SIMULATION

| Specimen ID | (G_F) in N/m from experiments | | | | | (G_F) in N/m from simulation | | | |
|-------------|--------------------------------------|---------|----------------|---|--|------------------------------------|---|------------------------------------|---|
| | $(G_F)e$ From P-CMOD curve in N/m | CV In % | $((G_F)_{AV})$ | $(G_F)v$ from P- δ curve in N/m | Ratio of $\frac{(G_F)v}{((G_F)_{AV})}$ | Smeared crack approach | | Discrete crack approach | |
| | | | | | | $(G_F)cs$ from P-CMOD curve in N/m | Ratio of $\frac{(G_F)cs}{((G_F)_{AV})}$ | $(G_F)cd$ from P-CMOD curve in N/m | Ratio of $\frac{(G_F)cd}{((G_F)_{AV})}$ |
| L-P-1 | 298.71 | 3.185 | 288.8 | 278.5 | 0.965 | 279.84 | 0.969 | 280.43 | 0.971 |
| L-P-2 | 280.54 | | | | | | | | |
| L-P-3 | 287.15 | | | | | | | | |
| M-P-1 | 255.02 | 2.456 | 248.5 | 238.3 | 0.959 | 236.83 | 0.953 | 232.35 | 0.935 |
| M-P-2 | 242.93 | | | | | | | | |
| M-P-3 | 247.52 | | | | | | | | |
| S-P-1 | 229.82 | 4.69 | 221.8 | 212.1 | 0.956 | 202.28 | 0.912 | 197.40 | 0.890 |
| S-P-2 | 210.07 | | | | | | | | |
| S-P-3 | 225.57 | | | | | | | | |

It is evident from the Table 7 that the total fracture energy G_F from experiments as calculated from load deflection curve by work of fracture method yields less compared to that obtained from load CMOD curves. This ratio of $\frac{(G_F)v}{((G_F)_{AV})}$ is the correction factor will be nearly 0.95 for all beam sizes.

$$C.F = \frac{(Fr \text{ energy from load-deflection curves } ((G_F)v)}{(Fr \text{ energy from load-deflection curves } ((G_F)_{AV})} = 0.95 \quad (5)$$

The presence of powder content in excess compared to aggregates and super plasticizer in appropriate quantity are responsible to produce a mix of better uniformity and compaction, there by producing the SCC material with strong interfacial bond.

Similarly, the G_F calculated from load CMOD curves of simulations by both discrete crack and smeared crack approach yields values nearer to each other. However, it is found that these values are smaller compared with that of experiments. The ratios of simulation to experiments ranges from 0.89 to 0.971. It is observed that the simulation load CMOD curves nearly fit with experimental curves except there is decrease in the peak loads in these simulation curves.

TABLE 8
 PERCENTAGE ERROR IN TOTAL FRACTURE ENERGIES IN N/M

| Beam series | Mean of experimental range | Smeared crack approach | Discrete crack approach | % error | |
|-------------|----------------------------|------------------------|-------------------------|---------|----------|
| | | | | Smeared | Discrete |
| L-P | 288.80 | 279.84 | 280.43 | 3.12 | 2.90 |
| M-P | 248.491 | 236.83 | 232.35 | 4.693 | 6.50 |
| S-P | 221.833 | 202.28 | 197.40 | 8.81 | 11.01 |

It is evident from **Table 8** that the total fracture energy G_F is size dependent property. As size of beam decreases, the total fracture energy as calculated by experiment and simulation using load CMOD curves reduces. The error in total fracture energy obtained by simulation compared to experimental values increases as the size of the beam reduces.

Further, the total fracture energy for normal concrete is usually the value around 100 to 120 N/m. However, in SCC, it is more than the double of this value. The other fracture parameters are also greater for SCC. This is due to strong interfacial bond of cement paste with rest of the matrix material maintaining the uniformity of matrix with better packing of ingredients due to the super plasticizer. As the strength of the SCC increases, still strong interfacial bond would be formed thereby increasing fracture energy. This is responsible to yield these results with less co-efficient of variation.

The peak loads are presented in **Table 9** below. It is observed that the mean of the peak loads obtained from load CMOD curves of simulation yields smaller than that obtained by experiments.

TABLE 9
 PERCENTAGE ERRORS IN PEAK LOADS IN KN

| Beam series | Mean of exptl range | Smeared crack approach | Discrete crack approach | % error | |
|-------------|---------------------|------------------------|-------------------------|---------|----------|
| | | | | Smeared | Discrete |
| L-P | 12.163 | 11.49 | 11.40 | 5.536 | 6.276 |
| M-P | 8.866 | 7.93 | 7.89 | 10.56 | 11.01 |
| S-P | 6.289 | 5.315 | 5.324 | 15.483 | 15.34 |

This difference of peak loads increases as the size of the beam decreases. As the size decreases, there will be decrease in peak load indicating the increasing ductility of the small size beams.

A. Establishment of Linear Regression Curve for the Total Fracture Energy

Using the experimental total fracture energy of the beams given in **Table 6**, a graph is developed as shown in **Fig 10** below.

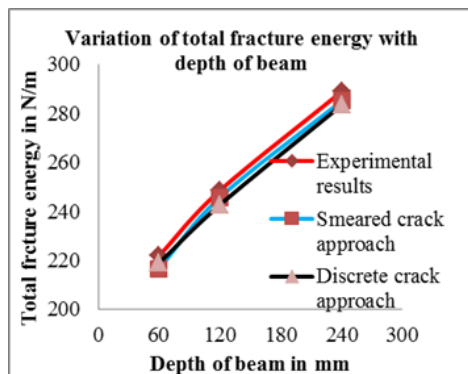


Fig 10: Variation G_F v/s Depth of beams

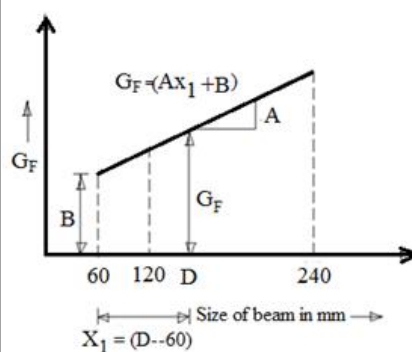


Fig 11: Variation of G_F v/s Size of beams

A linear regression line can be established for G_F with respect to the size of the beam by assuming that there is a linear variation of G_F with the size. This is shown in **Fig 11** above

This equation is as follows, $y = Ax_1 + B$ Where, $A = \left[\frac{(0.2888 - 0.2218)}{(240 - 60)} \right] = 3.722 * 10^{-04}$ and $B = 0.2218$ (6)

Hence, $y = (3.722 * 10^{-04}x_1 + 0.2218)$ and $G_F = [3.722 * 10^{-04}(D - 60) + 0.2218]$ (7)

Hence, using the above equation, the value of G_F can be established for any size beyond 60mm.

G. Determination of the Size Independent Specific Fracture Energy (G_F) for SCC Beams

The disadvantage of 3 point bending test (TPB) suggested by RILEM recommendations-1985 is that the total fracture energy (G_F) calculated using the complete area of load deflection curve by work of fracture method will be as the size dependent property instead of material dependent property. As size reduces, the fracture energy decreases. This disadvantage was investigated by many researchers.

Apart from the experimental errors caused due to testing equipment and setup, dissipation of energy in specimen bulk, the major error is with difficulties in capturing the tail part of load-deflection curves for beams especially for smaller beams.

Hence, loads at the tail end of the curves will not be continued till it reads zero value. At this stage, the true deflection/CMOD will not be maximum. The test may end prior to complete failure. In such case, the energy associated with self-weight depends on specimen weight and estimated load/CMOD value corresponding to the applied load at complete failure. Hence, the fracture energy estimated for self-weight (ΔG_F)_{tail} will be less than the actual one especially for smaller beams. If this complete failure of load-deflection/CMOD is captured for when the softening load reaches the point of zero force, the error in (G_F) of small beams can be avoided. However, the displacements/CMOD at low load levels may become unstable as the test approaches failure and thus the displacement at zero load may not be possible.

This problem, [21] (Elices. M., et al., 1992.) is solved by identifying the influence of cutting the P- δ tail end of load deflection curve. The tail end correction to obtain true value of total fracture energy was implemented. They introduced "A" which is the experimental co-efficient of adjustment of P- δ tail.

A method as proposed by M. Elices is also adopted by other researcher [22] (Hector Cifuentes et al., 2012) They also adopted Boundary Effect Method (BEM) suggested by Hu et al. to obtain size independent fracture energy (G_F). These methods were also followed by other researchers [23] (Ramachandramurthy et al., 2013)

A method adopted by University of Washington for modification in test method to measure total fracture energy (G_F) recommended by RILEM is followed by other researchers [24] (Joshua Martin et al., 2007). The test specimens were modified to include counterweights in an open loop testing machine. The use of counterweights allows stable testing to continue up to displacements much larger than that corresponding to loads. The resulting long tail of the load-displacement curve contributes to the total fracture energy. This accurate measurement contributed to the reduction in scatter of fracture energy values determined by RILEM procedure. Earlier to this attempt, Navalur et al. also adopted this method.

Hence, following the tail end correction method as suggested by M. Elices et al., the correction has been made to evaluate a unique value of (G_F) to consider it as a material dependent property. These are as follows.

Referring to the above **Table 7**, the size dependent (G_F) values based on load –deflection curves are considered. The load –vertical deflection (P v/s δ) values at the tail end of these curves were used to evaluate the following quantities.

Maximum moment M at the Centre of beam = $\left(\frac{PS}{4} \right)$ And, the corresponding rotation angle $\theta = \left(\frac{4\delta}{S} \right)$ (8)

Where, S is span of beam and δ is the central deflection.

Using these values, a graph of $\left(\frac{M}{t} \right)$ in Newtons v/s $\left(\frac{1}{\theta^2} * 10^5 \right)$ in $radians^{-2}$ are developed for all the three sizes of the beams. This graph is shown in **Fig 12** below.

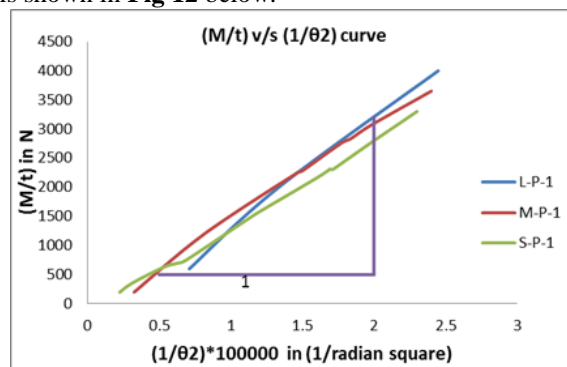


Fig 12: $\left(\frac{M}{t}\right)$ in N v/s $\left(\frac{1}{\theta^2}\right) * 10^5$ radians curves at tail end

The above graph is used to evaluate the experimental co-efficient of adjustment of P- δ tail 'A'. The 'A' is evaluated by taking the slope of a single interpolation line commonly passing through these three lines. Its value is estimated to be $(1800 * 10^{-5})$ N. Using 'A' value, fracture energies due to tail end $\Delta G_{F(tail)}$ are estimated in the **Table 10** as follows.

Hence, the size independent total fracture energy is the average of the above values for 3 beams = 342.3 N/m. Similarly, the load-CMOD curves can be used to determine specific fracture energy. However, this energy should be multiplied with C.F to evaluate true energy as per RILEM.

TABLE 10
 SPECIFIC FRACTURE ENERGIES FOR BEAMS

| Beam | G_F RILEM in N/m | Span 'S' in m | width of beam 't' in m | δ_f Deflection at mid span at test stop in mm | $(\Delta G_F)_{tail} =$ $\left(\frac{SA}{2\delta_f(D - a_o)}\right)$ In N/m | True G_F = $[G_F$ RILEM+ $(\Delta G_F)_{tail}$)] in N/m |
|-------|--------------------------|------------------|---------------------------------|--|---|---|
| L-P-1 | 278.5 | 0.96 | | 0.90 | 60 | 338.5 |
| M-P-1 | 233.3 | 0.48 | 0.1 | 0.50 | 108 | 341.3 |
| S-P-1 | 212.1 | 0.24 | | 0.40 | 135 | 347.1 |

B. To Determine Initial Fracture Energy (G_f) and Fracture Process Length (c_f)

Investigators such as Bazant et al.[1] (**Shah et al., 1995**) have introduced the valuable methods to determine the initial fracture energy (G_f). In this research work, the initial fracture energy (G_f) and fracture process length is (c_f) which is based on Size Effect Model (SEM) proposed by Bazant et al are determined as per RILEM for Span/Depth ratio of beams equal to 4. Using peak loads of load-CMOD curves of all three geometrically similar beams, a linear regression line of the form $Y = (A_B X + C_B)$ is plotted. The A_B is the slope of the line and C_B is intercept in the vertical direction. These parameters are determined using equations $G_f = \frac{[g(\alpha_o)]}{E A_B}$ and $c_f = \left[\frac{g(\alpha_o)}{g_1(\alpha_o)}\right] \left(\frac{C_B}{A_B}\right)$ where $g(\alpha_o)$ and $g_1(\alpha_o)$ are the geometric functions for Span/Depth ratio equal to 4 and $\alpha_o = \left(\frac{a_o}{D}\right)$.

It is observed from the results given in below **Table 11** that the ratio of $\left(\frac{G_F}{G_f}\right)$ from experimental load CMOD curves varies from 3.35 for L.P series to 2.88 for M.P. series and 2.57 for S.P series. As size of the beam decreases, the $\left(\frac{G_F}{G_f}\right)$ ratio also decreases.

TABLE 11
 COMPARISON OF G_f , G_F AND C_f

| Beam series | $(G_F)_{Av}$ In N/m | $(G_f)_{Av}$ $= \frac{K_{IC}^2}{E}$ in N/m | Experimental | | TPFM | | Smeared crack approach | | Discrete crack approach | |
|-------------|------------------------|---|--------------|-------------|--------------|-------------|------------------------|-------------|-------------------------|-------------|
| | | | G_f in N/m | c_f in mm | G_f in N/m | c_f in mm | G_f in N/m | c_f in mm | G_f in N/mm | c_f in mm |
| L.P | 288.8 | 91.45 | 86.33 | 18.72 | 91.45 | 9.06 | 84.07 | 25.5 | 82.12 | 24.83 |
| M.P | 248.5 | 97.22 | | | | | | | | |
| S.P | 221.8 | 95.55 | | | | | | | | |

The fracture process length (c_f) which depends on the size of the aggregates decreases, the brittleness also decreases. For normal concrete, its usual value is nearly 25mm. Its value for SCC with 20mm size aggregates is 18.72mm which indicates that SCC is more brittle compared to normal concrete. As c_f decreases, the brittleness of the material increases. However, its value drastically reduces to 9.06mm obtained by two parameter fracture models (TPFM), 25.5 mm by smeared crack approach and 24.825 mm from discrete crack approach.

Size Effect in SCC

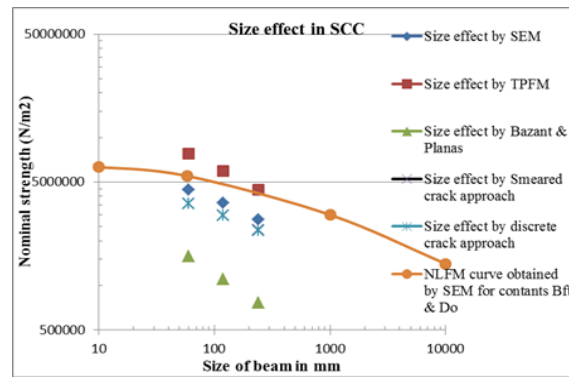


Fig 13: Size effect by all methods

The size effect is represented in the form of graph shown in **Fig 13** above. The values of Bf_t and D_o are calculated by using the peak loads of experimental load CMOD curves. It is evident from this graph that there will be the presence of size effect in SCC beams. As the size of the beam increases, there will be decrease in stress σ_N calculated by all the methods

J. Study of Brittleness Property:

The brittleness properties [1, 18] (Karihaloo, 1995) such as the characteristic length is calculated using $L_{ch} = \left(\frac{EGF}{f_t^2}\right)$, Material length by $Q = \left(\frac{ECTOD_c}{K_{IC}}\right)^2$ and β by $\left[\frac{Dg\left(\frac{a_0}{D}\right)}{c_f g\left(\frac{a_0}{D}\right)}\right]$ for L.P and M.P. series whereas by $\beta = \left[\frac{B^2 f_t g\left(\frac{a_0}{D}\right) D}{c_n E G f}\right]$ for M.P and S.P series and given in **Table 12** below.

TABLE 12
 CHARACTERYSTIC LENGTH, MATERIAL LENGTH & BRITTLENESS NUMBERS

| Beam | L_{ch} in mm | CV in % | Material length Q | CV in % | β range 0.1 to 10 |
|-------|----------------|---------|-------------------|---------|--------------------------------|
| L-P-1 | 643.10 | 3.185 | 99.474 | 14.64 | 4.146 |
| L-P-2 | 603.98 | | 85.16 | | |
| L-P-3 | 618.21 | | 74.29 | | |
| M-P-1 | 549.04 | 2.456 | 49.20 | 7.257 | $\beta=2.073$ $\beta=3.324$ |
| M-P-2 | 523.00 | | 55.709 | | |
| M-P-3 | 532.90 | | 49.295 | | |
| S-P-1 | 494.87 | 4.69 | 21.681 | 8.062 | 1.662 |
| S-P-2 | 452.26 | | 25.268 | | |
| S-P-3 | 485.632 | | 24.685 | | |

The degree of brittleness depends not only on intrinsic brittleness of concrete but also on the size of the structure. The brittleness is quantified by L_{ch}, c_f and Q. The trends in L_{ch}, c_f and Q are very similar. In a series of geometrically similar structure, as these values decrease, the brittleness decrease. The parameter β which depends on c_f is the only one which depends on the size of the beam. As β decreases, brittleness of the beam decreases. Brittleness is related to size effect. The results of brittleness number β as obtained by size effect law as $\left(\frac{D}{D_o}\right)$ or the other formula clearly shows that this number increases as size increases which clearly shows that the brittleness increases.

Hillerborg (1983) and Bache (1986) [18] (Karihaloo, 1995) proposed the ratio $\left(\frac{L_{ch}}{D}\right)$ as indicator of concrete structural brittleness, where D is the characteristic dimension of the structure. Carpinteri (1982) proposed the energy brittleness number S_e defined as $S_e = \left(\frac{G_F}{f_t} D\right)$. These values are calculated and presented in **Table 13** below.

TABLE 13
 BRITTLENESS PARAMETERS OF SCC BEAMS

| Beam series | D in mm | f_t in MPa | Average of L_{ch} in mm | $\frac{L_{ch}}{D}$ | Average of G_F In N/mm | S_e |
|-------------|---------|--------------|---------------------------|--------------------|--------------------------|----------|
| L-P | 240 | 4.24 | 621.76 | 2.591 | 0.2888 | 0.000284 |
| M-P | 120 | | 534.98 | 4.458 | 0.2482 | 0.000488 |
| S-P | 60 | | 477.59 | 7.960 | 0.2210 | 0.000872 |

It is evident from the above results that $\left(\frac{l_{ch}}{D}\right)$ and S_e increases as the size of the beam decreases. As these parameters increases their values for smaller size beams, the brittleness of the beam decreases.

K. Determination of the Kink Point.

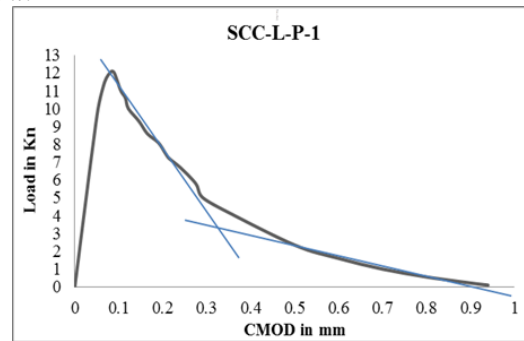


Fig 14: Kink point in P-CMOD curve

The co-ordinate of the kink point in failure envelope is found out in load CMOD curve. The softening curve after the peak load can be transformed into possible number of slopes as shown in **Fig 14** above. The intersection of these slopes itself is a kink point. The stress ratio at kink point is the ratio of load corresponding to kink point to that of the peak load in the curve

Referring the failure envelope curve for L-P-1 and from above curve,

$$\Psi = \left(\frac{\Psi f_t}{f_t}\right) = \left(\frac{\Psi P_u}{P_u}\right) = \left(\frac{3.50 \text{ KN}}{12.09 \text{ KN}}\right) = 0.289 \quad (9)$$

This procedure is repeated for the failure envelope curve of all the beams and represented in **Table 14** as follows.

TABLE 14
 STRESS RATIO Ψ AT KINK POINT FOR SCC BEAM

| Beam Id | $P_u = f_t$ In KN | $\Psi f_t = \Psi P_u$ In KN | Ψ_{Exptl} | CV in % | Ψ_{Av} | Ψ_{Smrd} | % error | Ψ_{Dis} | % error |
|---------|----------------------|--------------------------------|----------------|------------|-------------|---------------|------------|--------------|------------|
| L-P-1 | 12.09 | 3.50 | 0.289 | 2.31 | 0.282 | 0.29 | -2.84 | 0.274 | 2.91 |
| L-P-2 | 12.15 | 3.35 | 0.276 | | | | | | |
| L-P-3 | 12.25 | 3.45 | 0.282 | | | | | | |
| M-P-1 | 8.753 | 2.40 | 0.274 | 2.943 | 0.275 | 0.311 | -13.09 | 0.265 | 3.64 |
| M-P-2 | 8.861 | 2.37 | 0.268 | | | | | | |
| M-P-3 | 8.986 | 2.55 | 0.284 | | | | | | |
| S-P-1 | 6.305 | 1.70 | 0.269 | 2.37 | 0.272 | 0.301 | -10.66 | 0.279 | -2.574 |
| S-P-2 | 6.286 | 1.68 | 0.267 | | | | | | |
| S-P-3 | 6.275 | 1.75 | 0.279 | | | | | | |

L. Development of the Crack Model for SCC:

From the experimental Load CMOD curves, a non-linear fracture model can be developed for SCC. The bilinear softening model can be defined by the four experimental fracture parameters. These are hypothesis of the peak load of P-CMOD curve to the tensile strength (f_t), the area under the first slope of the softening curve to the initial fracture energy (G_f), the area under the whole curve is made equivalent to the total fracture energy (G_F) and the stress at kink point (Ψ) which is the ratio of load at kink point to the peak load of the experimental load CMOD curves. The three fracture parameters f_t , G_f and Ψ are the material dependent properties where as G_F is the size dependent property.

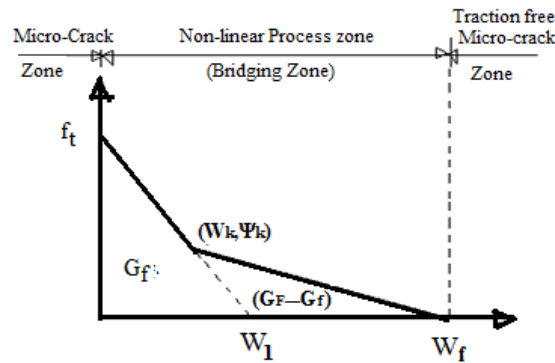


Fig 15: Bi-linear softening curve for SCC

From above **Fig 15**,

$$G_f = \left(\frac{1}{2}f_t w_1\right), \therefore w_1 = \left(\frac{2G_f}{f_t}\right) \text{ and, } G_F = \left[\frac{1}{2}f_t w_1 + \frac{1}{2}(w_f - w_1)\Psi f_t\right] \quad (10)$$

$$\text{And, } \left(\frac{f_t}{w_1}\right) = \left[\frac{\Psi f_t}{(w_1 - w_k)}\right] \text{ By re-arranging the this equation, We have, } \Psi = \frac{(w_1 - w_k)}{w_1} \quad (11)$$

$$\text{By re-arranging the above equation, } w_k = [w_1(1 - \Psi)] = \left[\left(\frac{2G_f}{f_t}\right)(1 - \Psi)\right] \quad (12)$$

Substituting the values of Ψ within the range 0.268 to 0.289 for any size of beam within the range taken, the value of w_k can be evaluated using the equation(13) as given above.

Equating the area under second slope of the softening curve, we get,

$$(G_F - G_f) = \left[\frac{1}{2}(w_f - w_1)\Psi f_t\right] \text{ and } w_f = \left[\left(\frac{2(G_F - G_f)}{\Psi f_t}\right) + w_1\right] = \left[\left(\frac{2(G_F - G_f)}{\Psi f_t}\right) + \left(\frac{2G_f}{f_t}\right)\right] \quad (13)$$

Knowing the numerical values of G_F, G_f, Ψ and f_t for the given beam, w_f can be calculated.

CONCLUSIONS:

- The load CMOD curves obtained by experiments and computer simulation using ATENA software will provide a better fit. The peak loads in simulation curves yields smaller than that obtained by experiments. The simulation of experimental load-CMOD curves can be predicted using ATENA software by both crack approaches.
- A bilinear crack model can be proposed for SCC and the model can be linked by the various fracture parameters (G_F, G_f, Ψ and f_t). An empirical method can be introduced to determine the stress ratio at kink point Ψ in the proposed model which can be directly calculated by taking the ratio of load at kink point to that of peak load in P-CMOD curve whose value ranges from 0.26 to 0.30 by both experiments and simulation.
- The $G_F, CTOD_c$ determined by RILEM procedure is proved to be size dependent property, since their values reduce as the size of beam reduces whereas the K_{IC} and G_f will be the material dependent properties. The G_F calculated from load deflection curve is 5% less than that obtained from load CMOD curves. As size of the beam decreases, the $\left(\frac{G_F}{G_f}\right)$ ratio decreases. The K_{IC} determined for SCC by LEM principle is found to be size dependent property since its value decreases for smaller beams.
- The method to determine G_F by tail end correction can be successfully adopted for SCC beams also to estimate the appropriate unique size independent specific fracture energy.
- The smaller value of $c_f = 18.72\text{mm}$ for SCC indicates that it is comparatively more brittle compared to the normal concrete whose value is usually 25mm.
- The presence of size effect is identified in SCC beams determined by different methods using experimental and simulation results.
- In a series of geometrically similar structure, the ductility of the SCC beams increases as its size decreases. This is identified by the decrease in the peak loads in the load CMOD/deflection curves, decrease in parameters L_{ch}, β and Q and increase in the parameters $\left(\frac{L_{ch}}{D}\right)$ and S_e as the size of the beam reduces.
- The fracture parameters can further be used as INPUT DATA in the ATENA software to study the mode of failure in various structures of chosen dimensions.

ACKNOWLEDGEMENTS

The author sincerely thanks the management and principal of Smt. Kamala and Shri. Venkappa. M. Agadi College of Engineering and Technology (SKSVMACET) LAXMESHWAR --582116, Dist: Gadag, Karnataka State for the support and encouragement given throughout the course of this work.

NOTATIONS

The following symbols are used in this paper.

| | |
|---------------|---|
| SCC-L-P-1,2,3 | Self-compacting concrete-Large size-Plain-Beam specimen no 1, 2 and 3 respectively |
| SCC-M-P-1,2,3 | Self-compacting concrete-Medium size-Plain-Beam specimen no 1, 2 and 3 respectively |
| SCC-S-P-1,2,3 | Self-compacting concrete-Small size-Plain-Beam specimen no 1, 2 and 3 respectively |

REFERENCES

- [1]. Shah.S.P., Swartz.S.E & Ouyang.C(1995) ,"A Text Book on Fracture Mechanics of Concrete: Application of Fracture Mechanics to Concrete, Rock other Quasi-brittle Material", Published by John Wiley and Sons. pp 117,137,144 and 146-156,164,175.173.
- [2] Raghu Prasad. B.K (1996), Professor, Department of Civil Engineering, IISc, Bangalore," Proceedings of the Q.I.P short term course on Fracture Mechanics of Plain and reinforced concrete " September 9 -14,1996, pp BKR II-8.
- [3].Jeffrey, Roesler., Glaucio.H.Paulino., Kyoungsoo, Park. & Cristian, Gaedick.,(2007) "Concrete fracture prediction using bilinear softening", Cement and Concrete Composites, Volume -29,2007,pp 300--312.
- [4].Jeffrey,Roesler,Glaucio,H.,Paulino,Kyoungsoo,Park.,&Cristian,Gaedick.,(2008) "Determination of the kink point in the bilinear softening model for concrete" , Engineering Fracture Mechanics, Volume 75, 2008, pp3806--3818.
- [5].Chao,Wang.,Yamei, Zhang.& Zhe, Zhao.,(2012) "Fracture process of rubberized concrete by fictitious crack model and AE monitoring", Computers and Concrete, Volume 9, No 1(2012),pp. 51-61.
- [6].Planas.J. Elices.M., Guinea.G.V., Gomez.F.J., Cendon.D.A., & Arbilla.I.,(2003)"Generalization and specifications of cohesive crack models", Engineering Fracture Mechanics, Volume 70, 2003,pp1759-1776.
- [7].Ricardo,A,Einsfeld.,Marta,S.L. & Velaso.,(2006) "Fracture parameters for high performance concrete" Cement and Concrete Research, Volume 36,(2006) , pp 576-583.
- [8]. Apparao, G.,& Raghu Prasad, B.K.,(2002) "Fracture energy and softening behavior of high strength concrete", Cement and Concrete Research, Volume-32(2002), pp 247-252.
- [9]. Cervenka, V. & Pukl, R.,(1995) "Sbeta analysis of size effect in concrete Structures", Proceedings of the second international conference on fracture mechanics of concrete structures,(FRAMCOS2):1387,1396,Ed.F.H.Wittmann,AEDIFICATIO,ETHZurich,1995,Switzerland.
- [10]. Zhifang, Zhao.,Seung, Hei, Kwon & Surendra, P.Shah.,(2008) "Effect of specimen size on fracture energy and softening curve of concrete, Part-I, Experiments and Fracture Energy", Cement and Concrete Research, Volume-38 (2008),pp. 1049-1060.
- [11].Okamura, H., &Ozawa, K.,(1994) "Self compactable HPC in Japan",SP169:1994,ACI,Detroit,1994,pp 31-44.
- [12]. EFNARC (European federation of national trade associations representing producers and applicators of specialist building product),(2002) "Specifications and Guidelines for self-compacting concrete", February-2002, Hampshire, UK.
- [13].Nan, Su. Hsu, K.C., & Chai, H.W.,(2001) "A simple mix design for self-compacting concrete" ,Cement and concrete Research, Volume 31(2001), pp1799-1807.
- [14]. Nagendra, R. & Sharadha Bai., (2013) "Self compacting concrete containing granite powder", Indian Concrete Journal, April 2013, pp22-26.
- [15]. Manu, Santhanam., & Subramanian.,(2004) "Current Developments in SCC", Indian concrete journal, June 2004,pp 11-21.
- [16]. H, Vijaykumar, & Sakey Shamu.,(2015)" A critical study on the influence of steel fiber on the performance of fresh and hard self-compacting concrete", Journal of Structural Engineering, Volume 42,No 3,August-September 2015,pp 237-245.
- [17]. Shetty, M.S., "A Text Book of Concrete Technology- Theory and Practice" Text Book published by Chand. S. and Company Ltd.
- [18]. Bushan,L,Karihaloo.,Text book on " Fracture Mechanics and Structural Concrete" ,Published by Longman Scientific and Technical ,England, First published 1995,pp 44,45,132, 208-281.
- [19].Eskandhari, H., Muralidhara, S., Raghuprasad.B.K &VenkataramaReddy.B.V, (2010) "Sadhana", Volume-35, Part-3, June 2010, pp 303-317, © Indian Academy of Science.
- [20]. Djamila, Benarbia., & Mohamed, Benguediab.,(2015) "Determination of stress intensity factor in concrete material under Brazilian disc and three point bending test using finite element method".Periodica polytechnic, Mechanical Engineering, September 2015,59(4),pp.199-203.
- [21].Elices, M., Guinea,G.V., &Planas.J.,(1992) "Measurement of the fracture energy using three point bend tests: Part 3-Influence of cutting the P- δ tail" Materials and Structures, 1992, 25, pp. 327-334.

- [22]. Hector Cifuentes, Maria Alcalde & Fernando Medina (2012) “Comparison of the size dependent fracture energy of concrete obtained by two tests” VIII international conference on fracture mechanics of concrete and concrete structures, Framcos-8.
- [23]. Ramachandramurthy.A., Karihaloo.B.L., Nagesh, R, Iyer & Raghuprasad. B.K., (2013) “Determination of Size Independent Specific Fracture Energy of Concrete Mixes by Two Methods”, Cement And Concrete Research, 2013, Volume-50, pp. 19-25.
- [24]. Joshua Martin, John Stanton, Nilanjan Mitra & Laura N Lowes (2007) “ Experimental testing to determine concrete fracture energy using simple laboratory set up” Technical paper in ACI Materials journal , November-December 2007, pp 575-584.

ABOUT THE AUTHOR

Dr. Vijayakumar. Halakatti is awarded PhD degree from VTU Belgaum, Karnataka state, India in the year 2018. He completed M.E (structures) from Gulbarga University and B.E (civil) from Karnataka University Dharwad. He has more than 27 years of teaching experience at undergraduate level as Lecturer, Senior Lecturer and Assistant Professor and Associate Professor at various colleges and universities in India. Presently he is working as Associate Professor, Department of Civil Engineering, SKSVMA Charitable Trust's Smt. Kamala and Shri. Venkappa. M. Agadi College of Engineering and Technology (SKSVMACET) LAKSHMESHWAR-582116 Dist: Gadag, Karnataka State, India. His areas of interest are finite element analysis and fracture mechanics of concrete and self-compacting concrete etc.

